CHINESE OPTICS LETTERS

Vol. 21, No. 3 | March 2023

Transverse mode interaction-induced Raman laser switching dynamics in a silica rod microresonator

Xueying Jin (金雪莹)[1*], Qinglin Fang (方青林)[1], Xin Xu (徐 昕)[1], Yu Yang (杨 煜)[2], Haoran Gao (高浩然)[1], and Haojie Xia (夏豪杰)[1]

[1] Anhui Provincial Key Laboratory of Measuring Theory and Precision Instrument, School of Instrument Science and Optoelectronics Engineering, Hefei University of Technology, Hefei 230009, China

[2] School of Electrical Engineering and Automation, Hefei University of Technology, Hefei 230009, China

*Corresponding author: xyjin007@hfut.edu.cn

Received August 2, 2022 | Accepted November 7, 2022 | Posted Online November 28, 2022

We investigate the mechanisms to realize the Raman laser switching in a silica rod microresonator with mode-interaction-assisted excitation. The laser switching can be triggered between two whispering gallery modes (WGMs) with either the same or distinct mode families, depending on the pumping conditions. The experimental observations are in excellent agreement with a theoretical analysis based on coupled-mode equations with intermodal interaction terms involved. Additionally, we also demonstrate switching of a single-mode Raman laser and a wideband spectral tuning range up to ~32.67 nm by selective excitation of distinct mode sequences. The results contribute to the understanding of Raman lasing formation dynamics via interaction with transverse mode sequences and may extend the microcavity-based Raman microlasers to potential areas in switchable light sources, optical memories, and high sensitivity sensors.

Keywords: nonlinear optics devices; Raman laser; microresonators.
DOI: 10.3788/COL202321.031407

1. Introduction

Stimulated Raman scattering (SRS) has been of considerable interest as a means of extending the spectral coverage of existing laser sources, especially to the mid-infrared (MIR) wavelength regime via the interaction between light and molecular vibrations. The frequency offset of Stokes light is dependent on molecular vibration frequency of the host material[1,2]. Recent development of microcavity-based Raman lasers with high quality factors and small mode volume has successfully achieved microscale Raman lasing with high compactness, low energy consumption, and wideband spectral range[3–7]. Microcavity-based Raman lasers have been experimentally realized in silica microcavities[8,9], silicon racetrack resonators[5,10], fluoride resonators[11,12], titanium-sensitized silica microresonators[13], and on-chip diamond resonators[4]. More recently, widely tunable Raman lasers have also been demonstrated in chip-integrated chalcogenide microresonators, rendering the microcavity-based Raman lasers very promising[14]. Such nonlinear microcavities are an attractive platform, allowing for potential applications as compact switchable laser sources, optical clocks, and spectroscopic sensing[15–19].

Despite this exciting progress, challenges remain in achieving control over photonic Raman lasers. In general, the discrete tunability of Raman lasers over ~100 nm was demonstrated by scanning the pump laser wavelength[3,4,10]. By introducing cascaded Raman lasing, this tuning range can be extended to the MIR region[20]. In addition, cascaded Raman scattering can induce Raman laser switching between two whispering gallery modes (WGMs)[17]. Several techniques, including injection pump power tuning[21], environmental temperature adjustment, and mechanical stretching[22], can indeed tune the lasing wavelengths. Yet, the fundamental mechanisms for control of Raman lasing action and formation dynamics have not been well understood. The switching behavior was always associated with WGMs of the same mode family. Since silica exhibits broadband Raman gain over 10 THz, and a silica rod microcavity supports plenty of mode families, the formation and switching dynamics of Raman lasing with a different mode family is highly desirable.

In this report, we show both theoretically and experimentally that transverse mode interaction can induce Raman mode switching in silica rod microresonators. The transition behavior between both the same and different mode families can be achieved by controlling the pump power. We employ a coupled-mode theory framework with additional intermodal interaction terms included to describe the physical mechanisms of Raman mode switching in this overmoded microcavity. Moreover, the single-mode Raman switching is also demonstrated to cover a

wavelength range of over 32 nm by adjusting the axial coupling positions. This study illustrates the importance of considering transverse mode interaction for Raman lasing in any microcavity with localized transverse modes.

2. Theoretical Model and Analysis

Figure 1(a) depicts the generation and switching principle of the transverse mode interaction-assisted multimode Raman lasing. The Raman light can be created in a WGM microcavity provided that these two conditions are satisfied: i) the frequency of high-Q modes coincides with Raman gain; ii) the mode overlap between the Stokes mode and the pump mode is sufficient. With a broadband, homogeneous Raman gain, a single pump can only excite one mode with the highest gain, owing to the gain-clamping effect in the cavity[23]. Nevertheless, in practical experiments, multimode Raman lasing usually occurs in a single-mode pumped microcavity even with a frequency spacing that is not an integer number of the free spectral range (FSR).

Consider that the Raman gain in silica has a broadband profile with a full width at half-maximum (FWHM) of ~10 THz[24], which corresponds to a continuum in frequency. Additionally, the silica rod resonators with a submillimeter scale thickness can support abundant WGM families. As a consequence, WGMs

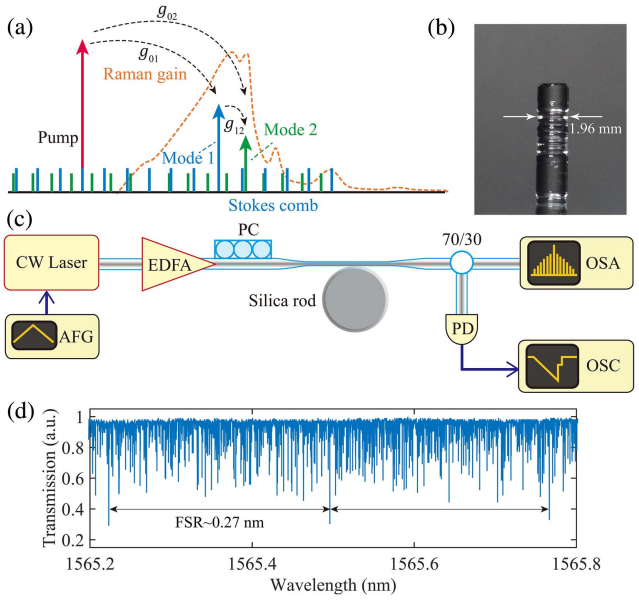

Fig. 1. Experimental scheme and methods of the proposed device. (a) Principle of Raman laser switching in a two-mode-family Raman laser; (b) experimental photograph of the fabricated WGM microrod cavity with a diameter of ~1.96 mm; (c) experimental setup and device for generation and switching of Raman lasers in a silica rod microcavity. CW laser, continuous-wave tunable laser diode; EDFA, erbium-doped fiber amplifier; PC, polarization controller; PD, photodetector; OSA, optical spectrum analyzer; OSC, digital storage oscilloscope; AFG, arbitrary function generator. A microfiber is exploited as an evanescent coupler to couple light in and out of the silica rod microcavity.

with distinct mode families may be simultaneously excited, and it is natural to introduce a coupling term between the multiple Stokes (Raman) modes. Here, we propose a mechanism to show that the presence of transverse mode interaction can modulate the Raman lasing dynamics effectively. As described in Fig. 1(a), two modes in the different mode families are initiated simultaneously by a single-mode pump. The two excited modes acquire their gain from the pumped mode, while in the meantime, the energy converts from Mode 1 to Mode 2 through intermodal interaction g_{12}. The strength of this interaction depends upon the mode overlap between two modes, and may play a delicate role in Raman laser switching dynamics.

To gain physical insight into the multimode Raman switching dynamics, we employ a modified coupled-mode equation, taking the transverse mode interaction terms into account. The calculation is utilized to acquire the dynamics of energy transition via SRS and transverse mode interaction. The jth cavity mode couples with the injection pump energy in the microfiber waveguide as well as all the other cavity modes through Raman scattering. The time evolution of the intracavity fields can be described as

$$\frac{\mathrm{d}E_j}{\mathrm{d}t} = -\frac{1}{2}\gamma_j E_j + \sum_{i<j} g_{ij}|E_i|^2 E_j - \sum_{k>j} g_{jk}\frac{\omega_j}{\omega_k}|E_k|^2 E_j + [\sqrt{\gamma_{\mathrm{ex}}}s_{\mathrm{in}}]_{j=0}. \tag{1}$$

Here E_j signifies the slowly varying amplitude for pump and Stokes cavity modes, and $P_{\mathrm{in}} = |s_{\mathrm{in}}|^2$ is the input pump power from the waveguide. γ_j and γ_{ex} are related to the total cavity decay rate and waveguide–resonator coupling rate, respectively, which are regarded as independent of mode number. ω_j denotes the resonant frequency of the excited mode. The intracavity nonlinear Raman gain coefficient is given by

$$g_{ij} = \frac{c^2}{2n^2}\frac{1}{V_{\mathrm{eff}}}g_R \qquad \text{and} \qquad V_{\mathrm{eff}} = \frac{\int |\vec{E}_p|^2 \mathrm{d}V \int |\vec{E}_R|^2 \mathrm{d}V}{\int |\vec{E}_p|^2 |\vec{E}_R|^2 \mathrm{d}V}, \tag{2}$$

where g_R is the nonlinear bulk Raman gain coefficient. c is the speed of light, and n refers to the refractive index of silica material. V_{eff} denotes the effective modal volume and depends upon the mode overlap between the two modes. $\vec{E}_p$ and $\vec{E}_R$ account for the electric field vectors of pump and Raman modes.

Here we consider a simplest case with a single pump mode and two Raman modes. The two Raman modes belong to two distinct transverse mode families. The intracavity fields in steady-state operation can be derived as

$$P_0\left(-\frac{1}{2}\gamma_0 - g_{01}\frac{\omega_0}{\omega_1}P_1 - g_{02}\frac{\omega_0}{\omega_2}P_2\right)^2 = \gamma_{\mathrm{ex}}P_{\mathrm{in}}, \tag{3}$$

$$P_1\left(-\frac{1}{2}\gamma_1 + g_{01}P_0 - g_{12}\frac{\omega_1}{\omega_2}P_2\right)^2 = 0, \tag{4}$$

$$P_2\left(-\frac{1}{2}\gamma_2 + g_{02}P_0 + g_{12}P_1\right)^2 = 0, \tag{5}$$

where P_0, P_1, and P_2 refer to the intracavity power of pumped mode, Raman Mode 1, and Raman Mode 2, respectively.

Figure 2 shows the lasing action and the corresponding four different steady-state regimes as a function of injection pump power P_{in}. We consider two mode families, TE_{00} and TE_{02}, in Figs. 2(a) and 2(c), and TE_{00} and TE_{10} in Fig. 2(d), which are present in our silica rod microcavity. The mode profiles that we use are shown in Fig. 2(b). The effective mode volume V_{eff} is calculated exploiting a mode solver based on the finite-element method. The diameter of the microcavity is 1.96 mm and the axial cavity profile is fitted with a parabola to match the fabricated rod cavity. The calculated results are $V_{effTE02-TE02} = 1.62 \times 10^6\ \mu m^3$, $V_{effTE00-TE02} = 2.76 \times 10^6\ \mu m^3$, $V_{effTE10-TE10} = 1.48 \times 10^6\ \mu m^3$, and $V_{effTE00-TE10} = 2.74 \times 10^6\ \mu m^3$. Mode 1 and the pumped mode belong to the same mode family, and thereby they have larger mode overlap and higher Raman gain coefficient. Hence, Mode 1 lases first once the gain exceeds its loss (Regime II), as depicted in Figs. 2(a), 2(c), and 2(d). It can be shown that P_1 increases with injection pump power P_{in}, while the power in pumped mode P_0 is clamped at $\gamma_1/2g_{01}$. As a consequence, Mode 2 cannot acquire sufficient gain from Mode 1 to start lasing. On another front, Mode 1 also offers a gain channel for Mode 2 through transverse mode interaction. The gain is proportional to the intracavity power of Raman Mode 1.

When the launched power is further increased, Mode 2 starts to lase owing to the simultaneous excitation by the pump and Raman Mode 1. With the emergence of Mode 2, Mode 1 is gradually suppressed, since Mode 2 opens a loss channel for Mode 1 via the Raman process. In this two-mode lasing regime (Regime III), the intracavity powers P_1 and P_2 obey the following linear relationship:

$$g_{01}P_1 + g_{02}\frac{\omega_1}{\omega_2}P_2 = \frac{g_{01}\gamma_2 - g_{02}\gamma_1}{2g_{12}}. \tag{6}$$

After a critical point, Mode 1 is completely turned off (Regime IV), as shown in Figs. 2(a), 2(c), and 2(d). With a further increase of injection pump power, Mode 1 cannot rise again, while the power of Mode 2 increases with P_{in}. This interesting phenomenon can be explained by the two following main reasons. First, the Q factor of Mode 1 decreases at the onset of Raman Mode 2 oscillation, due to the additional loss channel provided by the latter. Therefore, the threshold of Mode 1 is increased accordingly. Second, the gain supplied to Mode 1 remains constant, since the pump power experiences threshold clamping on account of Mode 2. The above calculations show a unidirectional energy transfer between two Stokes modes, and demonstrate that the weak transverse mode interaction can modulate the multimode laser dynamics effectively.

3. Experimental Results

To experimentally confirm the Raman laser switching, we implemented the measurements exploiting a silica rod microcavity with a diameter of ~1.96 mm. The silica rod microcavity with an unloaded optical quality factor over $\sim 10^8$ was fabricated by using CO_2 laser in the machining processes[25]. Light was

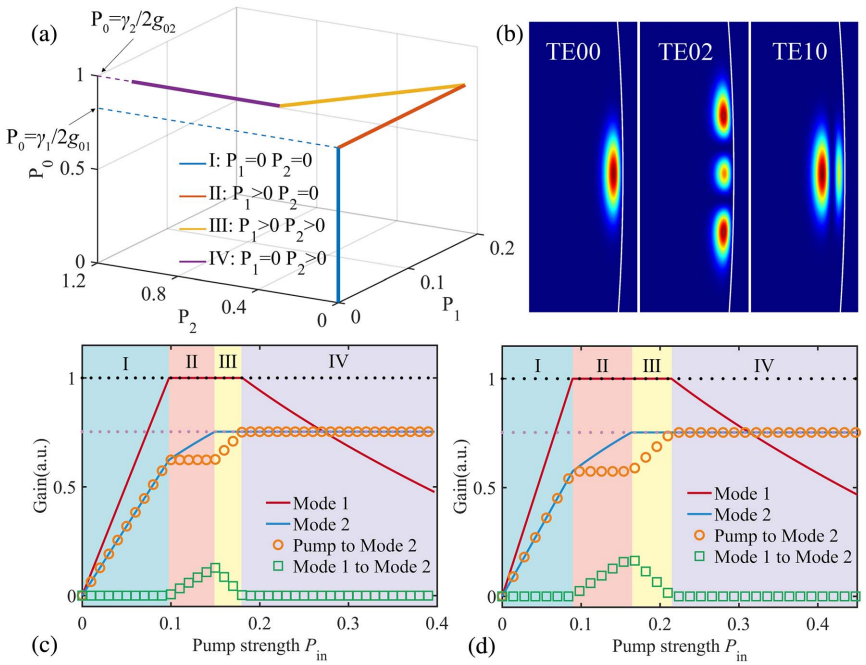

Fig. 2. Switching of multimode Raman lasing, calculated by using Eqs. (3)–(5). (a) Intracavity powers of pumped mode, Mode 1, and Mode 2 with the increase of injection power P_{in}; (b) calculated mode profiles for TE_{00}, TE_{02}, and TE_{10} modes in a silica rod microcavity using finite-element method; (c), (d) gain of two Raman modes from the pump and the other mode; The black (purple) dotted line represents the cavity loss of Mode 1 (Mode 2). We adopt TE_{02} (TE_{10}) for pumped mode and Raman Mode 1, and TE_{00} (TE_{00}) for Raman Mode 2 in panel (c) [panel (d)].

coupled from a CW pump laser (Toptica CTL 1550) into the microrod resonator through a tapered fiber [see Fig. 1(c)]. The output laser was then divided by a 70:30 splitter. The 30% arm output was sent to a photodetector (PD, Thorlabs PDA05CF2) connected to a digital oscilloscope (Keysight DSO 4054A) for monitoring the WGM transmission spectrum, while the 70% output was routed to an optical spectrum analyzer (OSA, Anritsu MS9740A) for observing the Raman lasing spectrum. The tunable CW pump was scanned from a short to a long wavelength and was thermally locked to excite the high-Q modes[26]. Figure 1(d) displays the mode spectrum of a microrod cavity. It is seen that, a series of axial modes are decoupled and situated within successive modes separated by the azimuthal FSR (~0.27 nm). The splitting of these transverse modes has essential consequences for the spectral features and dynamics of Raman laser emission.

First, we investigate the switching of Raman lasing between two modes, Mode 1 and Mode 2. Figures 3(a) and 3(b) show Raman laser dynamics by decreasing the detuning between the pump and resonance, which is equivalent to adjusting the cavity coupling power. The detuning is adjusted by scanning the pump wavelength with the help of a function generator. The pump wavelength and launched power are 1565 nm and 300 mW, respectively. The pump power used in our work is much larger than the Raman threshold reported in previous work[9], which can be attributed to the inevitably increased effective mode volume V_{eff}, and hence, the threshold of Raman lasers. The greatly increased V_{eff} results from large size of our rod cavity and the participation of multiple mode families in this Raman process. As the pump laser frequency approaches the resonance from its blue-detuned side, Mode 1 was first created at 1675.18 nm (State a), which belongs to Regime II in Fig. 2. Reducing the detuning caused a new peak emerging at 1684.9 nm (State b–State c). By further decreasing the detuning, the Stokes energy is gradually converted from Mode 1 to Mode 2, and the power switching occurred between two Raman modes (State d–State h). State d–State h can be classified into Regime III in Fig. 2. Eventually, Mode 1 was totally suppressed, and Mode 2 becomes the dominant peak (State i, Regime IV). Therefore, selective excitation of Raman lasing mode at Mode 1 or Mode 2 can be achieved by controlling the detuning. The Raman laser switching behavior was also demonstrated using another silica microrod cavity with a diameter of ~1.1 mm, as evidenced in Fig. 3(b). It is seen that the two-mode Raman lasing is surrounded by multiple four-wave mixing (FWM) peaks with an identical spacing of 1-FSR, which is caused by Raman-assisted FWM. The weak FWM peaks do not greatly influence the Raman switching behavior, since the unequally spaced Raman modes do not strongly interact through FWM process. Thus, our theoretical model, with no FWM involved, can describe the phenomena.

To further study the energy transfer between two lasing modes, we measured the output powers of Mode 1 and Mode 2 during the switching process, as shown in Fig. 3(c). With a

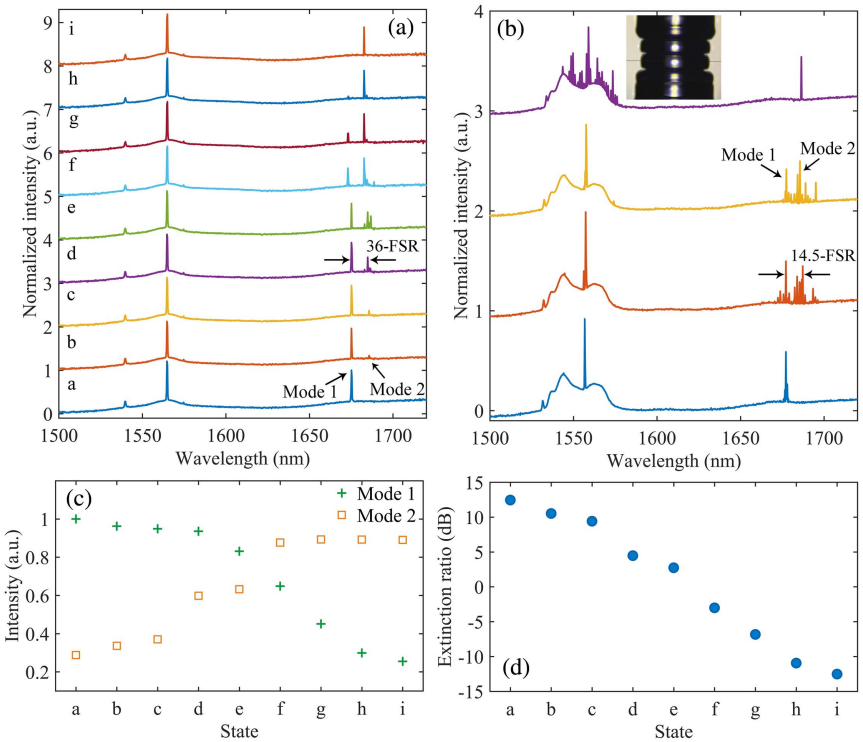

Fig. 3. (a), (b) Raman switching process between two modes while decreasing the detuning between the resonance and pump with a silica rod microcavity of (a) ~1.96 mm and (b) ~1.1 mm in diameter; inset, microscopic image of the silica microrod cavity; (c) output powers of Mode 1 (crosses) and Mode 2 (squares) for the nine states in (a); (d) extinction ratio of the two lasing modes in (a).

decrease of detuning, the powers of peaks at 1675.18 and 1684.9 nm cross over. The emission power of Mode 2 shows a slight growth with further reducing of detuning, while the Mode 1 exhibits a moderate drop. Figure 3(d) presents the corresponding extinction ratio of the spectra, which is defined as $10\log(P_1/P_2)$. The extinction ratio shows a nearly linear relationship from 12.5 to −12.5 dB with a decrease of detuning. It is worth noting that frequency spacings between the two lasing modes are integer multiples of FSR, i.e., 36-FSR for Fig. 3(a), while the frequency spacing is 14.5-FSR for Fig. 3(b). Hence, the two lasing modes do not belong to the same mode family for the latter case. The mode overlap is thereby required to be considered, which is important for Raman lasing at high powers[27]. Note that the transverse mode interaction may be suppressed owing to weak mode overlap, as it can lead to very large effective mode volume and small gain coefficient. The single-mode or two-mode oscillation can be extracted following the three-step procedure[28], that is, separating the Raman lasers from the pump with a 1550/1670-nm wavelength division multiplexer (WDM); selecting the target mode using a fiber Bragg gratings (FBG); and amplifying the mode by the injection-locking technique. Additionally, through heterodyning the frequency with a stabilized optical frequency source and measuring the beat signal, the linewidth and phase noise can be analyzed. With multiple lasing modes involved, the Raman switching behavior becomes more abundant, especially when the phase-matching condition is satisfied and other nonlinear effects take place at the same time. Detailed investigation and theoretical analysis of these complex phenomena are beyond the scope of this work.

Next, we explore the single-mode Raman switching by selective excitation of distinct transverse mode families. By changing the axial coupling position of tapered fiber relative to the microrod resonator, we observed switching between the single-mode Raman lasing, excited at Stokes frequencies corresponding to "jumps" by multiple or even fraction ratio FSR, as depicted by Fig. 4. During the process, the pump laser wavelength keeps almost unchanged, and the influence of radius change on FSR is nearly negligible. Note that the frequency spacing may not be an integer number of the azimuthal FSR, as the excited Raman lasing modes could belong to distinct transverse-mode sequences. For example, the frequency spacing between the last two Raman peaks is 25/3-FSR. The whole switchable range covers from 1659.52 to 1692.19 nm, corresponding to a wideband tuning range of 32.67 nm.

As is widely known, the Stokes modes belonging to another mode family form when the following two conditions are satisfied: Condition 1 is that they locate within the Raman gain provided by the pumped mode; Condition 2 is that the longitudinal mode separation or FSR of the Stokes mode family should match the pumped mode FSR. Therefore, the single-mode Raman switching phenomenon can be explained as follows. By adjusting the axial coupling position, modes with different axial mode numbers can be selectively created, which allows for the variations of group velocity dispersion (GVD)[29]. This means that they correspond to different FSR-matching wavelengths, and hence, the Raman lasing wavelengths can be manipulated flexibly by changing the tapered fiber coupling positions[6]. Although the detuning between the pump and resonance can also lead to single-mode Raman switching, we can simply rule it out, since it usually causes a frequency jump by fewer than three WGMs[30]. Compared with the mechanical- or temperature-switching methods[14,21,22], our approach achieved a broader tuning range by up to 1 order of magnitude.

Finally, we evaluated the stability performance of the generated Raman lasing. The created Raman lasing signal was well sustained in a harsh operation environment, i.e., at a pump power of 500 mW and without any temperature control device. In the regime of single-mode operation, Raman lasing oscillation was measured at room temperature for over 47 min with a sampling period of 0.5 min. Figure 5 shows that the stability of the Raman lasing intensity was in the range of −16.5% to 10% with a standard deviation of 5.82%, which corresponds to an intensity fluctuation of 3.36 μW. The variation in Raman lasing powers can be traced back to temperature fluctuations in the silica. First, it modifies the Raman shift and leads to variations of generated Stokes lasing intensities, since the Raman gain is frequency-dependent. Second, it causes a mode shift owing to the thermo-optic and thermal expansion effect, which

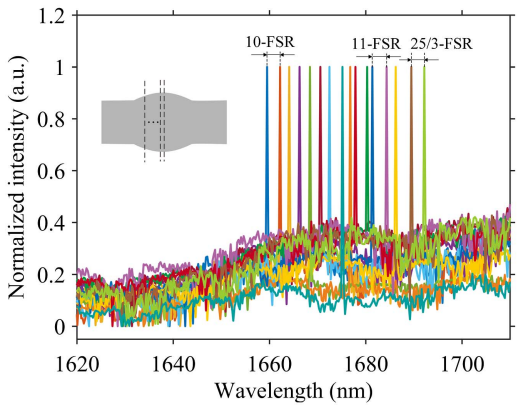

Fig. 4. Experimental switching of single-mode Raman lasing with different axial mode families; the Raman offset transits from 1659.52 to 1692.19 nm. The pump wavelength and launched pump power are 1551 nm and 300 mW.

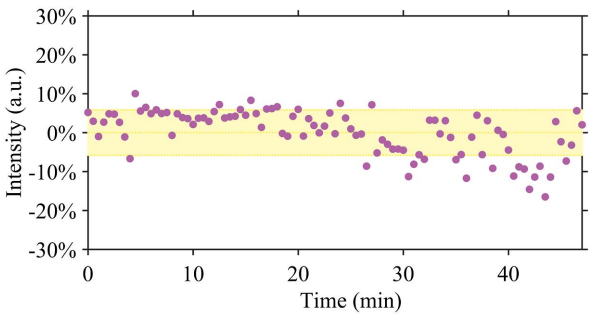

Fig. 5. Intensity stability of the Raman laser emission over 47 min for Stokes frequency excited at 1672 nm; the colored area indicates the standard deviation from the mean value.

substantially influences the coupling efficiency of the created Raman mode. Although we did not monitor the wavelength stability due to the limited resolution of the OSA, one may expect the Raman laser to be relatively stable with a narrow linewidth considering our device is a millimeter-scale cavity[31].

4. Discussion and Conclusion

In summary, we have investigated the Raman laser switching in a centimeter scale silica microrod cavity. We show that, aside from modification of local dispersion, interaction between spatial modes has a significant impact on Raman lasing dynamics and multimode switching behavior. The Raman energy conversion from Mode 1 to Mode 2 can be controlled via detuning adjustment. A theoretical analysis exploiting a coupled-mode equation, taking intermodal interaction processes into account, supports the experimental observations. Furthermore, we demonstrated a single-mode Raman switching by selective excitation of distinct mode series, with a shift that is 1 order of magnitude larger than that of thermal/mechanical tuning method. Compared to previous studies where Raman laser switching is realized with two competing split modes[32], our mode-interaction-based switching approach not only removes the need for finding split Raman modes that can be well-resolved, but also enlarges the beating frequency range of the two lasing modes.

This study provides an understanding of the Raman lasing formation dynamics, which may play an important role in realization of phase-locked Raman lasers, Kerr comb generation, and Stokes soliton generation. In particular, in the application of nanoparticle detection with a Raman mode-splitting scheme, the coexisting multiple lasing modes belonging to different mode families have distinct spatial field distributions, and thus provide different response for a binding particle/molecule[33,34]. Hence, our scheme can enlarge the spatial detection range and avoid missing a binding nanoparticle that may be undetected if only one lasing mode is employed. Therefore, Raman mode switching assisted by transverse-mode interaction may provide a strategy for applications such as wavelength-switchable light sources, all-optical memories, and optical sensors.

Acknowledgement

This work was supported by the National Natural Science Foundation of China (No. 62005071), the Natural Science Foundation of Anhui Province (No. 2008085QF312), the Fundamental Research Funds for the Central Universities (No. JZ2021HGTB0079), and the National Key Research and Development Program of China (No. 2019YFE010747).

References

1. X. Shen, H. Choi, D. Chen, W. Zhao, and A. M. Armani, "Raman laser from an optical resonator with a grafted single-molecule monolayer," Nat. Photon. **14**, 95 (2020).
2. Z. Gong, M. Li, X. Liu, Y. Xu, J. Lu, A. Bruch, J. B. Surya, C. Zou, and H. X. Tang, "Photonic dissipation control for Kerr soliton generation in strongly Raman-active media," Phys. Rev. Lett. **125**, 183901 (2020).
3. X. Liu, C. Sun, B. Xiong, L. Wang, J. Wang, Y. Han, Z. Hao, H. Li, Y. Luo, J. Yan, T. Wei, Y. Zhang, and J. Wang, "Integrated continuous-wave aluminum nitride Raman laser," Optica **4**, 893 (2017).
4. P. Latawiec, V. Venkataraman, M. J. Burek, B. J. Hausmann, I. Bulu, and M. Lončar, "On-chip diamond Raman laser," Optica **2**, 924 (2015).
5. Z. Zhou, B. Yin, and J. Michel, "On-chip light sources for silicon photonics," Light Sci. Appl. **4**, e358 (2015).
6. X. Jin, Y. Yang, X. Xu, K. Wang, L. Yu, and H. Xia, "Broadband manipulation of Stokes Raman frequency combs via mode division multiplexing in optical microcavities," J. Light. Technol. **40**, 5141 (2022).
7. Z. Dong, Y. Song, R. Xu, Y. Zheng, J. Tian, and K. Li, "Broadband spectrum generation with compact Yb-doped fiber laser by intra-cavity cascaded Raman scattering," Chin. Opt. Lett. **15**, 071408 (2017).
8. R. Suzuki, A. Kubota, A. Hori, S. Fujii, and T. Tanabe, "Broadband gain induced Raman comb formation in a silica microresonator," J. Opt. Soc. Am. B **35**, 933 (2018).
9. T. J. Kippenberg, S. M. Spillane, D. K. Armani, and K. J. Vahala, "Ultralow-threshold microcavity Raman laser on a microelectronic chip," Opt. Lett. **29**, 1224 (2004).
10. M. Ahmadi, W. Shi, and S. LaRochelle, "Widely tunable silicon Raman laser," Optica **8**, 804 (2021).
11. G. Lin and Y. K. Chembo, "Phase-locking transition in Raman combs generated with whispering gallery mode resonators," Opt. Lett. **41**, 3718 (2016).
12. G. Lin, A. Coillet, and Y. K. Chembo, "Nonlinear photonics with high-*Q* whispering-gallery-mode resonators," Adv. Opt. Photonics **9**, 828 (2017).
13. N. Deka, A. J. Maker, and A. M. Armani, "Titanium-enhanced Raman microcavity laser," Opt. Lett. **39**, 1354 (2014).
14. D. Xia, Y. Huang, B. Zhang, P. Zeng, J. Zhao, Z. Yang, S. Sun, L. Luo, G. Hu, D. Liu, Z. Wang, Y. Li, H. Guo, and Z. Li, "Engineered Raman lasing in photonic integrated chalcogenide microresonators," Laser Photonics Rev. **16**, 2100443 (2022).
15. Z. Li, Q. Du, C. Wang, J. Zou, T. Du, K. A. Richardson, Z. Cai, J. Hu, and Z. Luo, "Externally pumped photonic chip-based ultrafast Raman soliton source," Laser Photonics Rev. **15**, 2000301 (2021).
16. M. Yan, L. Zhang, Q. Hao, X. Shen, X. Qian, H. Chen, X. Ren, and H. Zeng, "Surface-enhanced dual-comb coherent Raman spectroscopy with nanoporous gold films," Laser Photonics Rev. **12**, 1800096 (2018).
17. S. Kasumie, F. Lei, J. M. Ward, X. Jiang, L. Yang, and S. Nic Chormaic, "Raman laser switching induced by cascaded light scattering," Laser Photonics Rev. **13**, 1900138 (2019).
18. P. Zhao, Y. Zhang, L. Wang, K. Cao, J. Su, S. Hu, and H. Hu, "Measurement of tropospheric CO_2 and aerosol extinction profiles with Raman lidar," Chin. Opt. Lett. **6**, 157 (2008).
19. K. Yang, H. Li, H. Gong, X. Shen, Q. Hao, M. Yan, K. Huang, and H. Zeng, "Temperature measurement based on adaptive dual-comb absorption spectral detection," Chin. Opt. Lett. **18**, 051401 (2020).
20. H. Rong, S. Xu, O. Cohen, O. Raday, M. Lee, V. Sih, and M. Paniccia, "A cascaded silicon Raman laser," Nat. Photon. **2**, 170 (2008).
21. B.-S. Moon, T. K. Lee, W. C. Jeon, S. K. Kwak, Y.-J. Kim, and D.-H. Kim, "Continuous-wave upconversion lasing with a sub-10 W cm^{-2} threshold enabled by atomic disorder in the host matrix," Nat. Commun. **12**, 4437 (2021).
22. Y. Chen, Z.-H. Zhou, C.-L. Zou, Z. Shen, G.-C. Guo, and C.-H. Dong, "Tunable Raman laser in a hollow bottle-like microresonator," Opt. Express **25**, 16879 (2017).
23. T. Carmon, T. J. Kippenberg, L. Yang, H. Rokhsari, S. Spillane, and K. J. Vahala, "Feedback control of ultra-high-*Q* microcavities: application to micro-Raman lasers and micro-parametric oscillators," Opt. Express **13**, 3558 (2005).
24. R. H. Stolen, J. P. Gordon, W. J. Tomlinson, and H. A. Haus, "Raman response function of silica-core fibers," J. Opt. Soc. Am. B **6**, 1159 (1989).
25. P. Del'Haye, S. A. Diddams, and S. B. Papp, "Laser-machined ultra-high-*Q* microrod resonators for nonlinear optics," Appl. Phys. Lett. **102**, 221119 (2013).
26. G. Lin, Y. Candela, O. Tillement, Z. Cai, V. Lefèvre-Seguin, and J. Hare, "Thermal bistability-based method for real-time optimization of ultralow-threshold whispering gallery mode microlasers," Opt. Lett. **37**, 5193 (2012).

27. O. Lux, S. Sarang, O. Kitzler, D. J. Spence, and R. P. Mildren, "Intrinsically stable high-power single longitudinal mode laser using spatial hole burning free gain," Optica **3**, 876 (2016).
28. H. Jang, B. S. Kim, B. S. Chun, H. J. Kang, Y. S. Jang, Y. W. Kim, Y. J. Kim, and S. W. Kim, "Comb-rooted multi-channel synthesis of ultra-narrow optical frequencies of few Hz linewidth," Sci. Rep. **9**, 7652 (2019).
29. G. Lin and Y. K. Chembo, "On the dispersion management of fluorite whispering-gallery mode resonators for Kerr optical frequency comb generation in the telecom and mid-infrared range," Opt. Express **23**, 1594 (2015).
30. A. V. Andrianov and E. A. Anashkina, "Single-mode silica microsphere Raman laser tunable in the U-band and beyond," Results Phys. **17**, 103084 (2020).
31. I. S. Grudinin and L. Maleki, "Efficient Raman laser based on a CaF_2 resonator," J. Opt. Soc. Am. B **25**, 594 (2008).
32. P.-J. Zhang, Q.-X. Ji, Q.-T. Cao, H. Wang, W. Liu, Q. Gong, and Y.-F. Xiao, "Single-mode characteristic of a supermode microcavity Raman laser," Proc. Natl. Acad. Sci. U.S.A. **118**, e2101605118 (2021).
33. B.-B. Li, W. R. Clements, X.-C. Yu, K. Shi, Q. Gong, and Y.-F. Xiao, "Single nanoparticle detection using split-mode microcavity Raman lasers," Proc. Natl. Acad. Sci. U.S.A. **111**, 14657 (2014).
34. Ş. K. Özdemir, J. Zhu, X. Yang, B. Peng, H. Yilmaz, L. He, F. Monifi, S. H. Huang, G. L. Long, and L. Yang, "Highly sensitive detection of nanoparticles with a self-referenced and self-heterodyned whispering-gallery Raman microlaser," Proc. Natl. Acad. Sci. U.S.A. **111**, E3836 (2014).